Weather and Climate Extremes 48 (2025) 100764

Contents lists available at ScienceDirect

Weather and Climate Extremes

journal homepage: www.elsevier.com/locate/wace

Sub-hourly precipitation and rainstorm event profiles in a convection-permitting multi-GCM ensemble

Marie Hundhausen [a,*], Hayley J. Fowler [b], Hendrik Feldmann [a], Joaquim G. Pinto [a]

[a] Institute of Meteorology and Climate Research, Troposphere Research (IMKTRO), Karlsruhe Institute of Technology (KIT), Karlsruhe, Germany
[b] School of Engineering, Newcastle University, Newcastle-upon-Tyne, UK

ARTICLE INFO

Dataset link: https://opendata.dwd.de/climate_environment/CDC

Keywords:
Sub-hourly precipitation
Extreme precipitation
Convection-permitting model
Multi-model ensemble
Regional climate modelling
COSMO-CLM

ABSTRACT

Extreme precipitation on short, sub-hourly time scales has the potential to trigger flash floods, is a particular threat to urban areas, and is expected to increase with climate change. However, little is known about sub-hourly precipitation extremes in convection-permitting climate models (CPMs). We investigate sub-hourly precipitation in the KIT-KLIWA ensemble — a CPM climate ensemble driven by 3 CMIP5 GCMs coupled to the regional climate model COSMO-CLM. The domain is centred over Germany with a grid resolution of 0.025° (2.8 km). In an event-based analysis, we compare extreme precipitation down to 5-min resolution for a historical simulation (1971–2000) with the dense radar and raingauge observation network in Germany. We find that 5-min CPM precipitation data adequately reproduces the frequency distribution from radar measurements. To improve the understanding of the precipitation bias in CPM simulations we propose an event-based analysis, that reveals a tendency for the CPM to overestimate the occurrence of longer events, and for a simulation bias in the representation of heavy and short, likely convective, precipitation events. The CPM historical simulations mostly reproduce the event precipitation sum for events leading to 1 h and 6 h annual maxima. Maximum 5-min peak intensities of these extreme precipitation events agree with spatially-aggregated radar data but are well below intensity maxima observed in station data. A dominant (very) front-loaded shape for precipitation events leading to 1 h annual maxima is reproduced by the CPM ensemble. The demonstration that CPMs effectively capture the key features of rainstorm profiles, opens up opportunities for climate change studies and their application in hydrological modelling.

1. Introduction

The intensification of extreme precipitation in a warming climate in Europe is projected to be largest for events of short duration (e.g., Rajczak and Schär, 2017; Helsen et al., 2020; Ban et al., 2015; Hundhausen et al., 2024). This prospect is a major concern because such events have the potential to trigger flash floods (Archer and Fowler, 2018). Their short response time, rapid water level rise and high peak depths lead to a high mortality (Archer and Fowler, 2018) and cause significant damage, especially in urbanized areas (Darwish et al., 2018). Besides the rainfall depth, the impacts of such extreme events are influenced by their temporal profile, including the timing of the peak and the peak intensity (Hettiarachchi et al., 2018; Lambourne and Stephenson, 1987; Müller et al., 2017; Ng et al., 2020; Zhu et al., 2018), which often occur on sub-hourly time scales.

In hydrological modelling for engineering applications, a single centred design rainfall profile, such as the Chicago Design Storm — is commonly used to drive an impact model to estimate a design flow (Villalobos Herrera et al., 2023a). Design rainfall profiles are typically based on ranked analytical approaches using long observational time series. However, a recent observational analysis in the UK suggests that real storms have a number of different temporal profiles — front-loaded, centred and back-loaded, whose frequency depends on storm duration (Villalobos Herrera et al., 2023a). Currently, it is assumed the same design profile(s), based on past observations, can be used in a warming climate. However, there are indications that the temporal profile is changing with climate conditions. For example, based on observations in Australia, storms have become more peaked (Wasko and Sharma, 2015) and more front-loaded (Visser et al., 2023) in the last decades. This poses a significant challenge for design flow estimation, which will be essential for successful climate adaptation. Accurately representing sub-hourly time scales precipitation characteristics, including the temporal profiles of extreme precipitation events, in climate models is crucial for providing adjustments to storm profiles for climate adaptation and for increasing the confidence in predicted climate change signals.

* Corresponding author.
E-mail address: marie.hundhausen@kit.edu (M. Hundhausen).

https://doi.org/10.1016/j.wace.2025.100764
Received 11 March 2024; Received in revised form 26 March 2025; Accepted 28 March 2025
Available online 10 April 2025

The new generation of climate model simulations at the convection-permitting (CP) scale, with a grid spacing of ≤ 4 km that permits the explicit resolution of deep convection, has been shown to improve the representation of precipitation. These improvements comprise especially the intensities and frequencies of extreme precipitation, the diurnal cycle and orographically-enhanced extreme precipitation (Kendon et al., 2012; Hohenegger et al., 2008; Sato et al., 2009; Prein et al., 2013; Ban et al., 2014, 2021). However, previous CPM studies analysing extreme precipitation have often been limited to daily or, less frequently, hourly model output, and little is known about sub-hourly extremes (Meredith et al., 2020).

Therefore, here we investigate sub-hourly precipitation in the KIT-KLIWA ensemble — a CP climate ensemble driven by four CMIP5 GCMs coupled to the regional climate model COSMO-CLM (Hundhausen et al., 2023). The domain is centred over Germany, with a grid resolution of 0.025 ° (2.8 km). For three ensemble members, we compare extreme precipitation of a temporal resolution down to 5-min during the historical simulations (1971–2000) with the dense observation network over Germany, representing the most comprehensive, and the only multi-model, study of sub-hourly precipitation in convection-permitting climate ensemble to date. While common analytical approaches remove the natural temporal correlation structure of precipitation events, we use an event-based approach to improve our understanding of the precipitation bias in CPM simulations and examine the representation of (sub-hourly) characteristics of rainstorms in CPM historical simulations.

The study addresses three research questions:

- How well are 5-min precipitation frequencies represented in a CPM simulation compared to observations?
- Can an event-based rainfall analysis improve our understanding of the precipitation biases in CPM simulations?
- What are the characteristics of extreme events and how are they represented in CPM simulations?

The paper is structured as follows: Section 2 provides a description of the data and methods used. Section 3 presents the results corresponding to the three research questions and additionally details the event-based analysis of precipitation event in 3.2. The discussion and conclusions are provided in Section 4.

2. Data and methods

2.1. The convection-permitting climate model ensemble

In the convection-permitting climate model (CPM) simulations of the KIT-KLIWA ensemble (Hundhausen et al., 2023) the following four CMIP5 GCMs were downscaled (realization in brackets): EC-EARTH (r12i1p1), HadGEM2-ES (r1i1p1), MPI-ESM-LR (r1i1p1), and CNRM-CM5 (r1i1p1). This downscaling was performed using the regional climate model COSMO5.0-CLM9 (Consortium for Small-scale Modelling Climate Limited-area Modelling; CCLM; Rockel et al. (2008)) and for three nesting steps. The first nest over Europe has a grid resolution of 0.44 ° (approximately 50 km), the intermediate nest over central Europe has a 0.0625 ° resolution (approximately 7 km), and the innermost nest covers central and southern Germany, as well as the Alpine area, with a 0.025 ° resolution (approximately 2.8 km). Convection is parametrized using the Tiedtke scheme (Tiedtke, 1989) for the first two nests, and for the innermost domain, this parametrization is applied only to shallow convection. Details regarding the nesting can be found in Hundhausen et al. (2023). The model results for the convection-permitting domain are hence referred to as the driving GCM with a -C appended.

The CPM simulation domain consists of 322 by 328 grid points. To mitigate boundary effects, the analysis domain excludes 48 grid points from each boundary. In addition, the southern boundary of the analysis domain was chosen so that it excludes the Alps, thereby avoiding regions with very complex orography, and the western boundary was aligned with German territory (Fig. 1). The analysis is limited to the German part of the domain to match the available observational data coverage. Previous studies, such as those by Brisson et al. (2015), support the chosen width of the truncated boundary zone as sufficient for spatial spinup. Furthermore, the nesting ratio of 2.5 is quite small, which further reduces the risk that convective cells do not have sufficient time to develop before they arrive at within the analysis domain. However, small domain sizes cannot ensure that influences from the coarser parent domain on the CPM simulation are excluded, especially for weather patterns with strong synoptic forcing (e.g. Prein et al., 2013). The climatological output fields for temperature and precipitation were evaluated for boundary effects, and the selected sponge area effectively minimized these effects, with no anomalies detected within the evaluation domain. Previously, successful CCLM simulations in the study region with a similar setup were performed on even smaller domains (Fosser et al., 2015; Hackenbruch et al., 2016). The added value of the 2.8 km resolution compared to the 7 km resolution in the KIT-KLIWA ensemble was assessed for temperature (Hundhausen et al., 2023) and precipitation (Hundhausen et al., 2024).

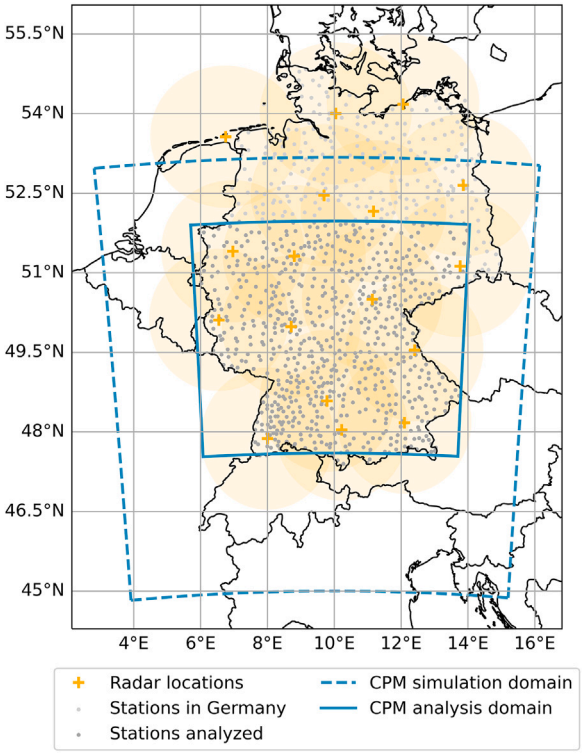

Fig. 1. Simulation domain and data coverage of the measurements. Yellow shading shows the theoretical coverage of the 17 radars. (For interpretation of the references to colour in this figure legend, the reader is referred to the web version of this article.)

Each simulation is transient from 1971–2100 using the RCP8.5 emission scenario. Sub-hourly, 5-min, precipitation is available for three ensemble members EC-EARTH-C, HadGEM2-ES-C, and MPI-ESM-LR-C for the historical period, 1971–2000. In the projection period, 5-min data is transiently available to 2100 for MPI-ESM-LR-C and for selected time slices for EC-EARTH-C and HadGEM2-ES-C. The analysis within this paper is limited to the historical period in EC-EARTH-C, HadGEM2-ES-C, and MPI-ESM-LR-C.

2.2. Sub-hourly observation data

Two 5-min datasets are used as a observational reference for the historical simulation (Table 1). The first is an *in-situ* precipitation

Table 1
Data coverage of the two observation datasets with 5-min resolution over Germany.

Data	Resolution	Period	Missing data
Stations	725 stations	first stations since 1995, data until 2022	16 years of data coverage in average, 8.6% missing data for operating stations
Radar	1 km×1 km raster	2003–2022	1.3%

dataset provided by the German weather service, Deutscher Wetterdienst (DWD). In Germany, precipitation stations with 5-min resolution have been operated since 1995; today there are 1008 5-min stations, from which 725 stations are located in the model domain (Fig. 1). The quality control of the measurements is carried out by the DWD and only quality-controlled data and years with >80% data completeness are used. The average available data length for the 725 stations used is 16 years. Secondly, we use the radar dataset, Radolan, provided by the DWD on a grid with a resolution of 1 km × 1 km (Bartels et al., 2004). Radolan provides 5-min resolution precipitation over Germany from 2000, and is a composite of 17 radars today (Fig. 1). The correction of the radar data and the transformation of the raw data into precipitation is performed by the DWD (Bartels et al., 2004). Due to the sparse data coverage in the first years of operation, the present study only analyses data for the 20 years from 2003 to 2022. For this analysis, the radar data are interpolated conservatively to the model grid at 0.025° (2.8 km) resolution. The interpolated data are hereafter referred to as the "radar model grid". As in the simulations, the interpolated radar data are analysed only over Germany to match the station measurements and to avoid sparse data coverage outside of Germany. For gridded radar data the maximum missing data per year and grid cell was restricted to 5%. In addition, radar data are analysed at the original resolution of 1 km × 1 km as nearest neighbours (grid cell) to the station locations and only for the years available at the respective station, to allow a direct comparison between the two datasets (notation "radar station grid").

2.3. Event-based analysis method

In an event-based analysis, a rain event is defined as a series of rainfall recordings separated from the next event by a sufficiently long rain-free period, which is referred to as the storm inter-arrival time. To avoid an arbitrary definition, this minimum rain-free period is estimated based on the consideration that the onset of independent rainstorms follows a Poisson process, meaning that the occurrence of one event does not affect the probability another event will occur. Intervals between the events are by theory distributed exponentially (Restrepo-Posada and Eagleson, 1982). Following Villalobos Herrera et al. (2023a), the minimum inter-arrival time was determined iteratively until rainstorm arrival times were exponentially distributed. Radar and CPM simulation grids were evaluated on a sparse matrix of every 50th grid point only due to computational resources. The sub-sample is assumed to be representative of the full grid. To ensure comparability of the different datasets, a constant inter-arrival time was then chosen across all datasets. The average radar value on the model grid of 7.5 h was chosen, as a compromise to best represent all datasets (see detailed results for the estimation of the inter-arrival time in Section 3.2).

To avoid including very long rainfall events with a large dry fraction, a two-step approach was implemented for event selection. In the first step, small, isolated peaks (below 1 mm) were set to zero. Therefore, an "almost-dry-window" with a duration of 7.5 h is applied as a running filter to the time series. Thus, all windows with less than 1 mm precipitation in 7.5 h are set to zero, and, to ensure to not cut off the tail or front of a rainfall event, the condition was imposed that precipitation has to be zero directly adjacent to the main event (for gridded data, the threshold for no rain was set to <0.01 mm, as very small values of precipitation occur in the time series) and ≤0.05 mm in the 1 h before/after an event to be considered as almost-dry-window. In the second step, event selection is performed on the filtered time series. Events are identified as precipitation recordings separated by an inter-arrival time of 7.5 h in the filtered time series. Step two is based on the code by Pichler (2024). The two-step procedure is illustrated in Supplementary Fig. S1. As shown in Fig. 2, for the 2016 flood event in southern Germany in the Braunsbach catchment (e.g., Piper et al., 2016), the almost-dry-window removes individual peaks before and after the event and reduces the rainfall event to a reasonable length.

In a third step, four event characteristics are calculated as shown in the example (Fig. 2). Event duration refers to the time from the first to last 5-min rainfall recorded during the event. The event sum describes the total rainfall summed over the entire duration of the event. The maximum peak intensity of an event is described as the maximum 5-min rainfall recorded. The temporal profile or shape of an event is parametrized by the D50 value, which is the percentage of the event's duration at which 50% of the cumulative precipitation sum of the event is reached (from Visser et al., 2023). Events with a small D50 describe a front-loaded event, while events with a large D50 describe a back-loaded event. We further refer to events with a D50≤20% as very front-loaded, 20%<D50≤40% as front-loaded, 40%<D50≤60% as centred, 60%<D50≤80% as back-loaded, and D50>80% as very back-loaded.

In order to assess the features of extreme events, the characterization of rainfall events is restricted to events that generate annual maxima (AM) of 1 h and 6 h duration. These AM-containing events are selected for each grid point (for CPM simulations and interpolated radar data) or station location (station measurement and radar) as the rainfall events that contain the annual maximum.

3. Results

3.1. Sub-hourly precipitation frequency

The frequency distributions of the precipitation datasets are analysed from the precipitation sum over a running window of the 4 different durations of 5 min, 15 min, 1 h and 6 h. The distributions shown are composite over all stations or grid points. The analysis shows high occurrence of low intensity rainfall and a decreasing occurrence with increasing intensity (Fig. 3a–d). Comparing the two observational datasets, there is good agreement between the station and radar observations for low to moderate rainfall intensities (Fig. 3a–b). The radar data shows a lower frequency of high and extreme intensities compared to the station measurements for all aggregations. This is particularly the case for short aggregations. In general, this difference can be attributed to the different characteristics of the datasets: while stations provide point measurements, the radar output is a gridded dataset and thus representative for an, albeit limited, area. As expected for a short temporal resolution, local high-intensity rainfall bursts, captured by local, point-like measurements, provide higher extreme values, in contrast to the larger spatial aggregations of rainfall provided by radar products.

In general, the CPM ensemble members reproduce the shape of the observed rainfall frequency curves and there is close agreement of the frequency distributions within the ensemble members (Fig. 3a–d). A systematic bias in the overestimation of low intensities compared to observations is apparent across all temporal resolutions from 5 min to 6 h. For the extremes, the model bias differs dependent on the temporal aggregation. Extreme values in the 5-min simulations mainly agree with the results of the radar measurement, while using a temporal resolution of 6 h, there is an overestimation of extreme intensities compared to the

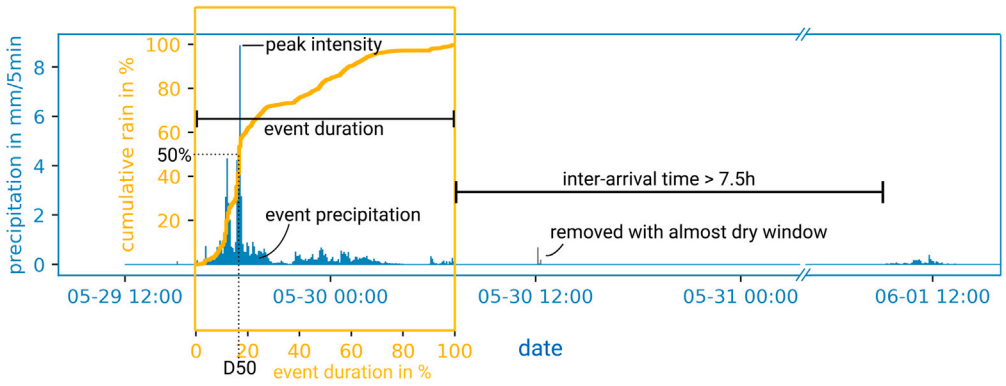

Fig. 2. Example event analysis for the DWD station Kupferzell-Rechbach during the flood event in the Braunsbach catchment in 2016. The detected rainfall event extends over the yellow box. Grey precipitation records are filtered out by the almost dry window. The event characteristics of event duration, peak intensity, event precipitation, and D50 are shown in the schematic. (For interpretation of the references to colour in this figure legend, the reader is referred to the web version of this article.)

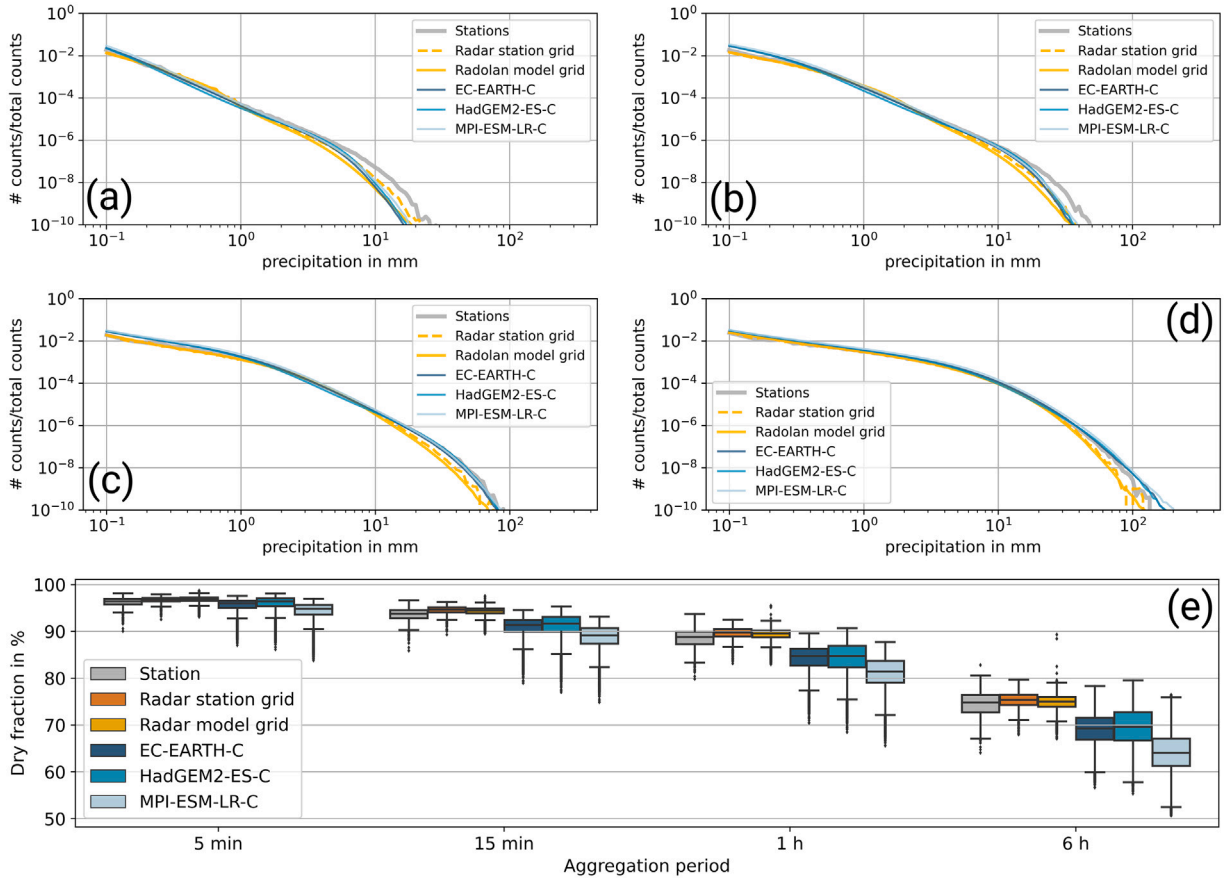

Fig. 3. Normalized frequency distribution for observational datasets and CPM simulation outputs over all grid points/stations in the evaluation domain for 5-min (a), 15-min (b), 1-h (c), and 6-h (d) durations. Panel (e) shows the dry fraction in the respective datasets and durations. Samples with <0.05 mm within the aggregation period are defined as dry.

observations. Therefore, extreme precipitation intensities in the CPM simulations seem to increase in comparison to the observations for increasing temporal aggregation.

The percentage dry fraction is highest at the shortest temporal resolution of 5-min and decreases with increasing duration (Fig. 3e). Comparing the two observational datasets, the radar data show slightly higher dry fraction compared to the station data. This difference appears less pronounced at higher temporal resolutions. The coarser resolution radar dataset on the model grid (2.8 km × 2.8 km) shows a slightly lower dry fraction than the radar data on the station grid (1 km × 1 km). The differences result from both, the different spatial resolutions and the smaller number of locations sampled in the radar station grid. The CPM simulations show a systematically lower dry fraction compared to observations, with wet bias increasing with increasing temporal aggregation. MPI-ESM-LR-C shows the lowest dry fraction in the ensemble, which is consistent with the higher precipitation totals simulated in MPI-ESM-LR-C (cf. following Table 2).

Our analysis of precipitation frequencies in the CPM ensemble compared to observations indicates that the sub-hourly 5-min CPM outputs adequately reproduce the observed precipitation frequency distribution over Germany. Compared to the observations, modelled extreme intensities appear to increase with longer duration. This leads to an overestimation of extreme precipitation at low temporal resolutions. Our findings imply that the CPM precipitation bias depends

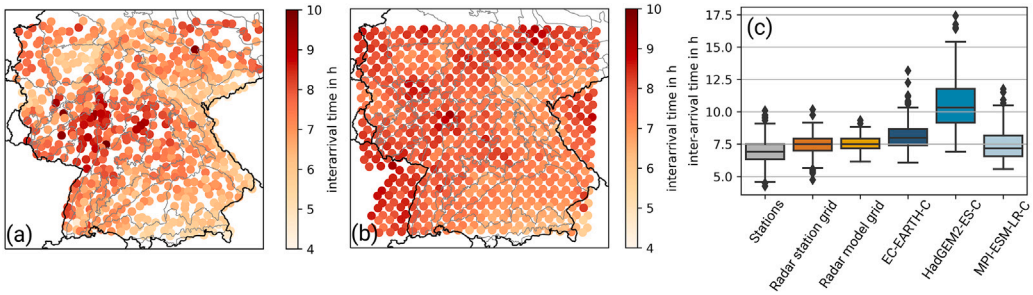

Fig. 4. Spatial distribution of the inter-arrival time in (a) station and (b) radar datasets. (c) shows the distribution of inter-arrival time over the German part of the domain for the observed datasets and the CPM simulations.

on the aggregation duration; this points towards a systematic bias in the temporal representation of rainfall events in the CP time series. We conclude therefore, that it is crucial to retain the natural temporal correlation structure of the precipitation sequence to evaluate the precipitation bias in CP simulations; thus, not using a typical ranked analytical approach. We propose to use an event-based analysis to help to improve the understanding of precipitation biases in CPM simulations.

3.2. Event-based analysis

Inter-arrival time. The minimum inter-arrival time over the study area shows a spatial pattern related to the altitude or the mean annual precipitation, which correlates with the former (Fig. 4a-b). The higher the altitude (or the higher the mean annual precipitation), the shorter the detected inter-arrival time. This observed spatial pattern is reproduced by the CPM ensemble members (Supplementary Information Fig. S2 and Fig. S3). The inter-arrival time in the station data is typically between 6.3 h to 6.9 h (25th and 75th percentile). The inter-arrival time for the radar dataset is significantly higher, from 7.2 h (7.0 h) to 7.9 h (7.9 h) (25th and 75th percentile for radar on model grid and for station grid in brackets) and shows lower overall variance. The spatial resolution of the radar data seems to have little effect on the result. The observations of inter-arrival time over Germany agree well with the results of Villalobos Herrera et al. (2023b) for south-west Britain, where they found an inter-arrival time predominantly between 6 and 9 h. CPM ensemble members EC-EARTH-C and particularly HadGEM2-ES-C tend to show higher inter-arrival times than the observations (Fig. 4c). MPI-ESM-LR-C has the shortest inter-arrival time in the CPM ensemble and therefore the best agreement with the observations. To enable comparability of the event-based analysis for the 6 datasets, a constant inter-arrival time was chosen for the analysis across all datasets. The average radar inter-arrival time of 7.5 h was chosen as a compromise to best represent all datasets.

Event distribution. An average of 800 mm precipitation per year accumulates in the station measurement data, of which 592 mm (74%) falls in events with a total of at least 5 mm of precipitation (Table 2). These rain events of at least 5 mm are hereafter referred to as significant events, thus excluding rain falling in the form of light showers or drizzle which contain only small amounts of precipitation that are presumably of little importance for the immediate hydrological response. Such significant precipitation occurs on average 43 times per year in the station measurements. The total annual precipitation is underestimated in the radar dataset compared to the *in-situ* measurements. The proportion of rain coming from significant events is also slightly lower (70%), with a similar range of 39 to 40 significant events per year (Table 2).

All CPM simulations overestimate total precipitation, which is a known bias for CPM (e.g., Prein et al., 2015). Depending on the forcing data, this overestimation varies strongly, with particularly high overestimation for MPI-ESM-LR-C (Table 2). The proportion of rain from significant events is from 76 to 80%, thus slightly higher in the CPMs than for observations. The EC-EARTH and MPI-ESM-LR driven runs show more significant events than observed. With 43 significant events per year, HadGEM2-ES-C is in agreement with the station measurements.

Significant events have most often relatively low intensities and their frequency decreases with event precipitation sum (Fig. 5). Significant event duration peaks at 6–9 h for the station measurements. Short-duration significant events are mainly associated with small event precipitation sums and their frequency decreases with event precipitation sum (Fig. 5). The distribution patterns of event precipitation sum and event duration are largely in agreement between the radar and station observations. The CPM simulations tend to have longer event durations than observations. Fig. 6 shows that the occurrence of short events is consistently underestimated in the CPM ensemble. The underestimation is strongest for short events with low precipitation totals. The occurrence of longer events however is overestimated by the CPMs.

Our results provide evidence that the precipitation bias in the ensemble CPM simulations is attributable to two factors. First, the occurrence of significant events seems to be overestimated in the CPM ensemble members that show strong total precipitation overestimates. Second, the event-based analysis reveals an underestimation of the proportion of short and small precipitation events, but a tendency to overestimate the occurrence of longer events. This finding suggests that the CPM ensemble members analysed here have deficiencies in reproducing significant short precipitation events, which are likely to contain significant convection.

3.3. Temporal profile characteristics of extreme events

The following section on the analysis of extreme events includes all events detected above that lead to an AM of either 1 h or 6 h duration at the respective station or grid point. Almost all of these 1 h (Fig. 7a) and 6 h (Fig. 7b) AM occur in the summer half-year (April to September). The peak of the observed AM occurrence is in June and July. The CPM simulations reproduce this seasonal pattern well, except for the ensemble member driven by HadGEM2-ES. We expect that due to a significantly too dry July in HadGEM2-ES-C compared to the observations, the probability of AM-generating rainfall in July is too low. The strong seasonality implies that the AM-generating events of interest analysed below are a sub-sample of events in the annual cycle, and the following characterization of AM extremes describes predominantly summer events.

The event duration of AM-generating rainfall extremes reaches from sub-hourly event duration to multi-day events (Fig. 7c,d). Comparing the two sets of observations for events leading to hourly AM, it is apparent that the larger the areal coverage of the measurement – from station data, a point measurement, to the radar on station grid (1 km × 1 km) to the radar on model grid (2.8 km × 2.8 km) – the lower the proportion of very short and short events (Fig. 7c). The same is seen for short events leading to 6 h AM (Fig. 7d).

Table 2
Annual mean precipitation for the different datasets over the model domain and overview of statistics for the event-based analysis.

Data	Precipitation in mm	Precipitation from events >5 mm in mm	number of events >5 mm
Stations	800	592	43
Radolan station grid	721	507	39
Radolan model grid	721	506	40
EC-EARTH-C	914	709	48
HadGEM2-ES-C	816	624	43
MPI-ESM-LR-C	1143	915	59

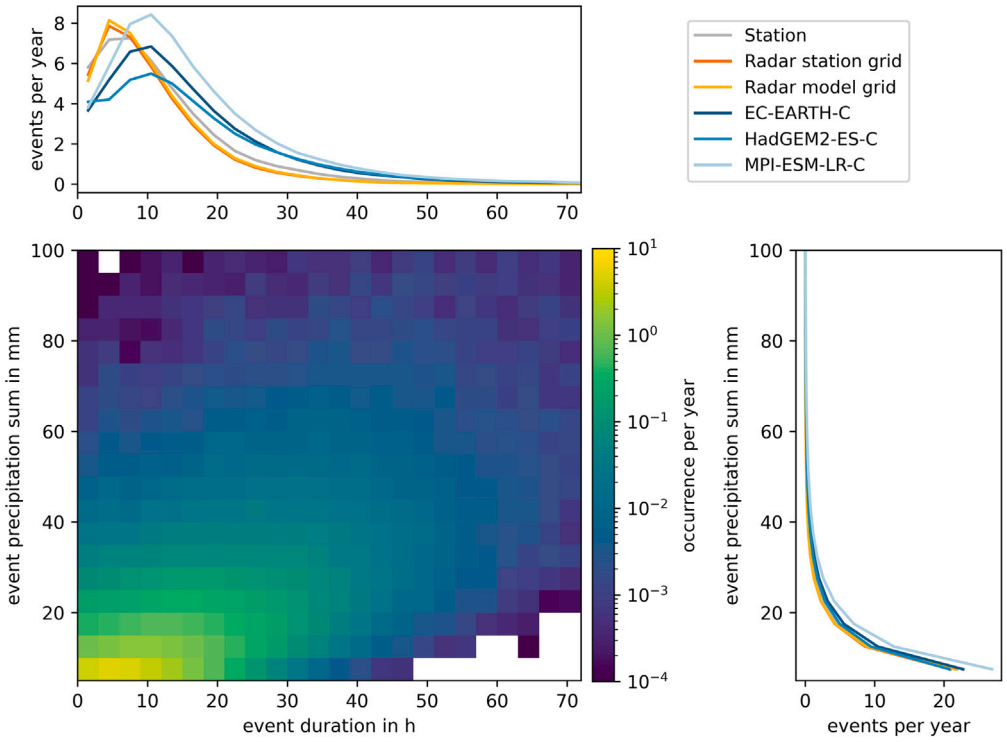

Fig. 5. The distribution of annual mean event frequency regarding event duration and event precipitation sum averaged over the station measurements is shown. The marginal distribution on the *x*-axis shows the respective frequency distribution for station, radar and the CPM ensemble members over the event duration, the marginal distribution on the *y*-axis shows the distribution over the event precipitation sum.

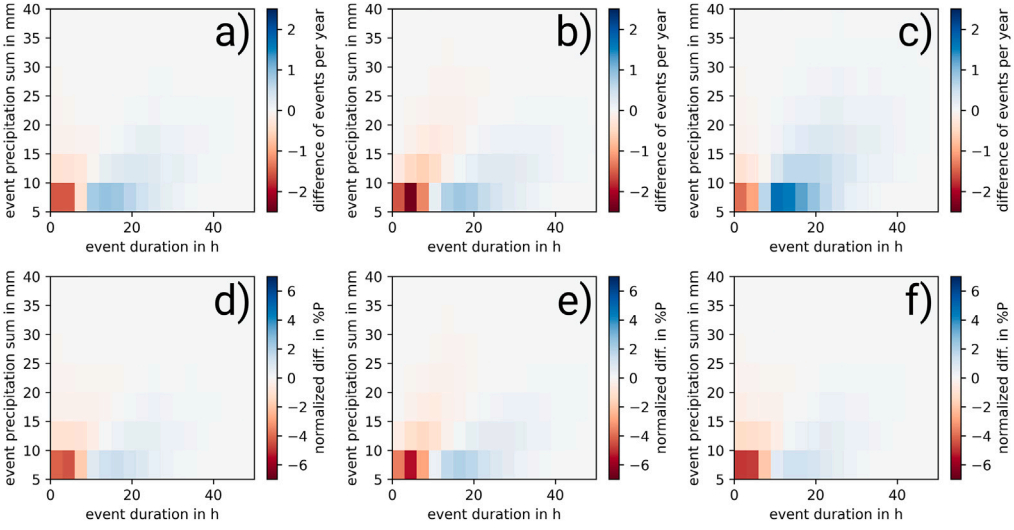

Fig. 6. The difference in event occurrence in the CPM simulations from the observed station distribution is shown in the first row for (a) EC-EARTH-C, (b) HadGEM2-ES-C, (c) MPI-ESM-LR-C. In the second row, the normalized differences in percentage points are shown for (d) EC-EARTH-C, (e) HadGEM2-ES-C, (f) MPI-ESM-LR-C. For the normalization, the mean annual event occurrence is scaled to 100% and the differences are displayed in percentage points. The respective comparison of station and radar observations in provided in the supporting information Fig. S4.

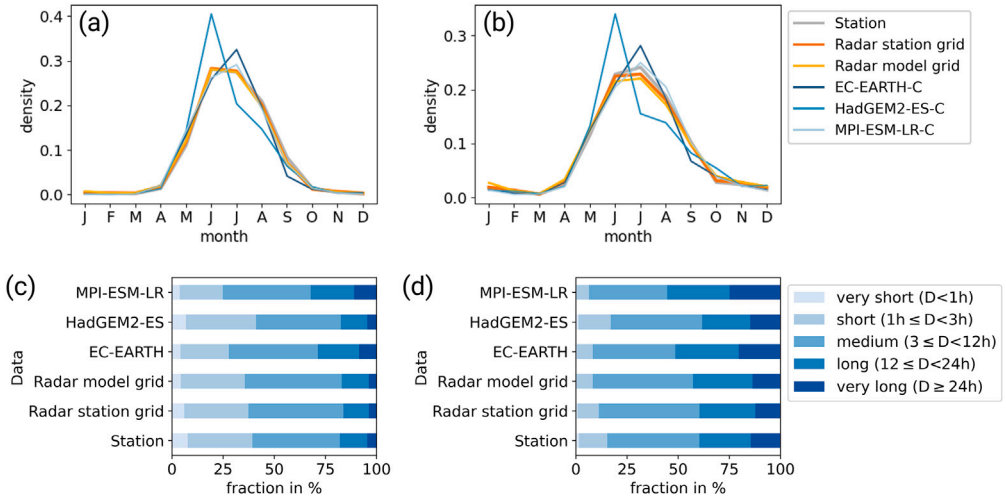

Fig. 7. The density distribution of AM-generating events over the year in the study area for 1 h-AM-generating events (a) and 6 h-AM-generating events (b) is shown. The distribution of the duration, divided into five sub-categories, of 1 h-AM-generating (c) and 6 h-AM-generating (d) events is shown on the bottom.

While the event durations in HadGEM2-ES-C are in good agreement with the station measurements for 1 h and 6 h AM-generating events, the CPM ensemble members MPI-ESM-LR-C and EC-EARTH-C underestimate the proportion of short events and overestimating the proportion of long events for 1 h AM-generating events compared to the observations. Since the CPM simulations produce average rainfall over a 2.8 × 2.8 km grid, the hypothesis is that they may under-represent the occurrence of short convective events or their intensities. We find that for 6 h AM-generating events, the proportion of short events is well represented in MPI-ESM-LR-C and EC-EARTH-C, but the occurrence of medium-length events is underestimated, and very long events are overestimated.

In order to ensure comparability between statistics, we divide extreme events into three sub-groups: short events (1 h to 3 h), medium-length events (3 h to 12 h) and long events (12 h to 24 h). These categories cover the majority of events. The small proportion of very short (<1 h) and very long (>24 h) extreme events are not considered due to lower data availability and hence large variance. We analyse event precipitation sum, peak intensity and D50 for the three duration categories (short, medium, long) based on the visualization of the characteristics of hourly (Fig. 8) and 6 h AM-generating events (Fig. 9).

Event precipitation sum. The event precipitation sum in the station data for 1 h AM-generating events (and 6 h AM-generating events in brackets) typically ranges from 17.1 to 29.4 mm (23.3 to 36.7 mm) for short events, from 22.2 to 38.0 mm (24.8 to 39.9 mm) for medium events, and from 29.0 to 42.9 mm (32.0 to 52.0 mm) for long events (inter-quartile range). Two relationships are apparent; the longer the event, generally the larger the event precipitation sum, and that events generating 6 h AM have generally more rain than 1 h AM-generating events. Both of these are reproduced by the radar observational datasets as well as by the CPM simulations (Figs. 8a–c and 9a–c). In general, the radar data shows lower event precipitation sums compared to the station measurements, especially for short and medium events, with a similar result, on the model grid (2.8 km × 2.8 km) and the station grid (1 km × 1 km). Only for short events generating hourly AM there is a visible difference between the two radar resolutions, with a higher event sum on the 1 km grid (Fig. 8a). The underestimation of event precipitation sums in the radar data compared to the station measurements is in accordance with an overall dry bias in the radar dataset (see Table 2).

There is generally good agreement within the CPM ensemble members. For 6 h AM-generating events, the event precipitation sum in MPI-ESM-LR-C is slightly higher than in EC-EARTH-C and HadGEM2-ES-C, which is in accordance with higher total annual precipitation in the MPI-ESM-LR driven simulation (see Table 2, Figs. 8a–c and 9a–c). The CPM simulations' event precipitation sum for short events and hourly AM is in good agreement with the station observations. The CPM simulations tend to overestimate the event precipitation sum slightly for medium events, and this overestimation is even stronger for long events. For 6 h AM-generating events there is a slightly more pronounced overestimation by the CPMs.

Peak intensity. A comparison of peak intensity in the different observational datasets shows a strong dependence on the measurement footprint (Figs. 8d–f and 9d–f). The 5-min peak intensity is lowest for the radar on model grid (2.8 km × 2.8 km), followed by the radar on station grid (1 km × 1 km) and highest values are in the station observations. The 95th percentile of 1 h (6 h) AM-generating events recorded by the station gauges is 12.8 mm (14.0 mm) for short events, 12.5 mm (12.0 mm) for medium events, 11.1 mm (9.2 mm) for long events. In addition to the effects of areal reduction, it is expected that the general underestimation of precipitation in the radar data compared to station data contributes to the bias in peak intensity.

The 5-min peak intensity distributions in the CPM simulations show good agreement within ensemble members. Although the 5-min peak intensities in CPM simulations are below the station measurements, they agree well with the 1 km × 1 km radar data, especially for the 1 h AM-generating events (Figs. 8d–f and 9d–f). Therefore, the CPM simulations of 5 min peak intensity are within the range of the two observational datasets.

D50. In the station data, the dominant fraction of 1 h AM-generating events is front-loaded (Fig. 8g–i). For 1 h AM-generating events, the longer the event, the more pronounced the peak at the very front-loaded end of the distribution. For 6 h AM-generating events, the D50 distribution for short events shows a similar distribution to the 1 h AM-generating events of mainly (very) front-loaded events (Fig. 9g–i). However, in the station measurements the proportion of (very) front-loaded events becomes smaller with increasing event duration of 6 h AM-generating events. The smallest fraction are very back-loaded events.

Comparing D50 in station and radar data, radar tends to show higher D50 and a lower fraction especially of very front-loaded events, with the largest differences found for short events. The D50 for radar on the station grid is generally within the distribution of the station and radar on the model grid for both 1 h and 6 h AM-generating events. We

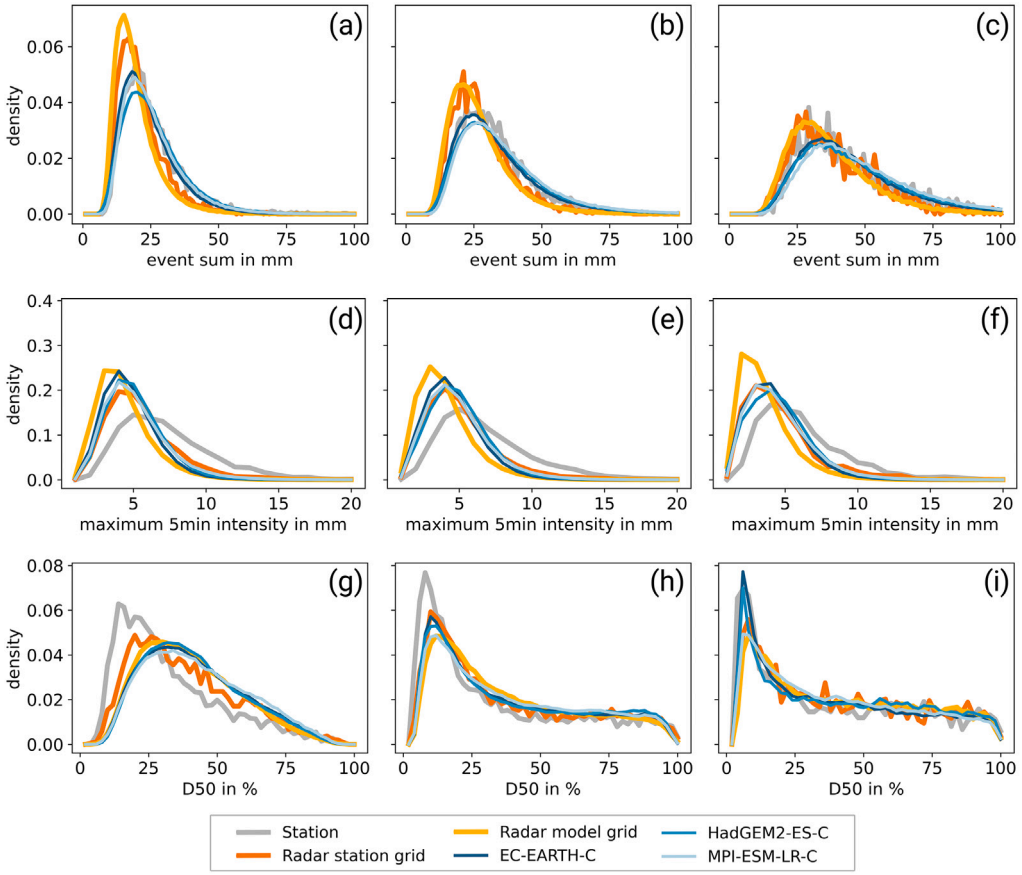

Fig. 8. Event precipitation sum (first row), maximum 5-min intensity (second row), and D50 (third row) for 1 h AM-generating events of different duration categories of short (first column), medium (second column) and long events (third column).

therefore attribute the bias, at least in part, to differences in the spatial footprint of the measurement.

A dominant (very) front-loaded fraction of events is reproduced by the CPM ensemble members with low ensemble spread. For short 1 h and 6 h AM-generating events, the CPM projections agree well with the radar on the model grid. For medium events, the CPM simulations appear to be in best agreement with the radar on the station grid, and are thus well within the range of radar and station observations (Figs. 8g–i and 9g–i). For long events, the ensemble spread is slightly higher and the agreement with both station and radar data, with a relatively similar distribution for long events, is good.

In summary, most 1 h and 6 h AM-generating events in southern Germany occur in summer. With an event duration typically ranging from 1 to 24 h, the AM-generating events are generally longer than the AM duration of 1 h. For 6 h AMs event durations shorter or longer than 6 h are common. Event precipitation sum in CPM simulations of AM-generating events is generally in good agreement with station measurements, but tends to be overestimated, especially for long events, which is consistent with the overestimation of precipitation totals in the CPM simulations. The maximum 5-min peak intensity in CPM simulations is in agreement with the radar data, but compared to station measurements the observed extreme intensities are not reached. A dominant (very) front-loaded fraction of events is reproduced by the CPM historical simulations and the probability distributions of D50 are mostly within the range of the station and radar observations.

4. Discussion and conclusions

In the presented study we investigate sub-hourly precipitation in a CPM climate ensemble for Germany and compare extreme precipitation down to 5-min resolution for the historical simulations (1971–2000) with the dense radar and raingauge observation network in Germany. A method for detection and characterization of precipitation event profiles was developed to improve the understanding of the precipitation bias in CPM simulations and in particular characterize extreme precipitation event leading to 1 h and 6 h annual maxima. We can draw three main findings:

1. 5-min CPM precipitation data adequately reproduces the observed precipitation frequency distribution, with an underestimation of the most extreme intensities compared to the station observations but in agreement with the radar data. However, for longer temporal aggregation (6 h) there is an overestimation of the most extreme intensities, revealing a mismatch of the precipitation temporal correlation structure.
2. The event-based analysis reveals an underestimation of the proportion of short and small precipitation events by the CPM, but a tendency to overestimate the occurrence of longer events. This implies that the CPM has deficiencies in reproducing likely convective, short precipitation events.
3. Events leading to 1 h and 6 h annual maxima in southern Germany mostly occur in summer and usually have an event duration between 1 and 24 h. CPM simulations generally reproduce event precipitation sums of those extremes of short and medium duration but tends to overestimate event precipitation sums for long events. Maximum peak intensity simulated by CPMs is in agreement with spatially aggregated radar data but well below intensity maxima in station data. A dominant (very) front-loaded fraction of extreme precipitation events leading to 1 h AM is reproduced by the CPM ensemble.

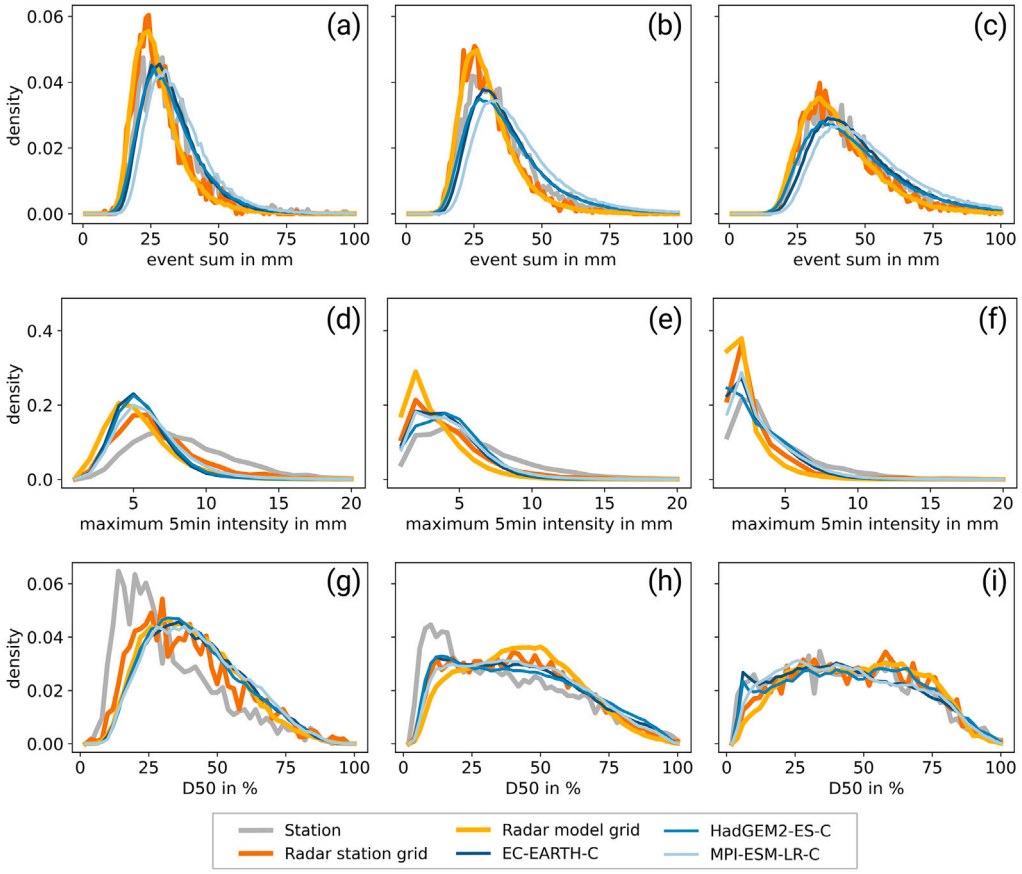

Fig. 9. Event precipitation sum (first row), maximum 5-min intensity (second row), and D50 (third row) for 6 h AM-generating events of different duration categories of short (first column), medium (second column) and long events (third column).

By investigating 5-min precipitation in a 30-year CPM simulation ensemble, we take a step towards closing the knowledge gap on sub-hourly CPM precipitation, an area where previous studies have been limited. Chan et al. (2016) derived climate change signals of sub-hourly precipitation from CPM projections, however no evaluation could be made due to lack of adequate observational data. The first evaluations of a sub-hourly CPM simulation compared to station observations were made with a decade-long COSMO-CLM simulation over Switzerland Vergara-Temprado et al. (2021), and a 22-year simulation over Barcelona (Meredith et al., 2020) that found adequate representation of precipitation on sub-hourly resolution and indications of a similar error in sub-hourly precipitation as for hourly resolution precipitation. With our study, we for the first time extended the analysis to a multi-GCM ensemble of CPM simulations and with a comparison with radar data in addition to station measurements. In the analysis of the 30-year historical period, we found that sub-hourly precipitation intensities are reasonably represented by the CPM simulations on a 0.025 ° (2.8 km) grid. The limitation of observations at high temporal resolution and the large observational range faced in the study constrains the validation of CPMs at high temporal resolution and, as emphasized by Chan et al. (2016), stresses the need for more quality-controlled high resolution observational data products.

We find a dependence of the bias for the extremes on the temporal resolution of the CPM simulation data, in agreement with Meredith et al. (2020). This bias leads to an overestimation of extreme precipitation intensities at low temporal resolutions. Based on this dependence of the precipitation bias on resolution, we conclude that it is crucial to preserve the natural temporal correlation structure of the precipitation sequence in the evaluation of the precipitation bias. Therefore, we propose an event-based analysis to improve the understanding of the precipitation bias in CPM simulations instead of typical ranked analytical approaches.

Event-based approaches have been applied previously on sub-hourly observational data, e.g. by Villalobos Herrera et al. (2023b), Visser et al. (2023), Wasko and Sharma (2015). For CPM data, the approach has been applied e.g. in Kendon et al. (2012), Fosser et al. (2015), Müller et al. (2023). However, these studies were limited to hourly data. The application of event-based analysis to multi-decade CPM 5-min outputs showed an underestimation of the proportion of short and small precipitation events by the CPMs, but a tendency to overestimate the occurrence of longer events. The overestimation of event duration is likely caused by low-intensity precipitation in the model, which aggregates precipitation episodes into excessively long events (Fosser et al., 2015). Moreover, the analysis indicates that the CPMs are deficient in reproducing strong and short, probably convective, precipitation events, in agreement with Kendon et al. (2012). The attribution of precipitation biases to events shows the potential for model development. In our application we were able to attribute errors to the forcing data, hence, for model development CPM simulations driven by reanalysis should be pursued.

Rainfall profiles of extreme events are of particular interest because of their importance for a range of practical applications. For engineering applications, such as urban drainage design, stress testing of infrastructure, and risk management, it is common to rely on design rainfall profiles, which are artificial profiles produced, often based on observations. Updating these profiles is clearly needed for resilient planning that considers future extreme events, given climate change and its potential changes on extreme precipitation. Realistic modelling of such extremes has been limited in the past by inadequate spatial resolution of climate models. Deep convection processes and related extremes in coarser climate simulations using parametrized convection

were found to be, in general too spatially diffuse, too persistent in time and showing too low intensity maxima of extremes (Kendon et al., 2012).

Our study shows that the characteristics of extreme precipitation events are well represented in a convection-permitting simulation. In particular, for AM-generating storms, the features of event precipitation sum, maximum peak intensity, and event shape are mostly within the observational range. Overall, the analysis of rainfall profile features shows that CPMs are able to represent the decisive features embedded in the design rainfall profiles, thus providing confidence in sub-hourly CPM simulations for future projections. This study is thus an important step towards the applicability of CPMs as a tool for studying future sub-hourly extreme precipitation, and paves the way for the application of CPMs for hydrological modelling in a warmer world.

CRediT authorship contribution statement

Marie Hundhausen: Writing – review & editing, Writing – original draft, Visualization, Methodology, Formal analysis, Conceptualization. **Hayley J. Fowler:** Writing – review & editing, Conceptualization. **Hendrik Feldmann:** Writing – review & editing, Funding acquisition, Data curation, Conceptualization. **Joaquim G. Pinto:** Writing – review & editing, Funding acquisition, Conceptualization.

Declaration of competing interest

The authors declare that they have no known competing financial interests or personal relationships that could have appeared to influence the work reported in this paper.

Acknowledgements

The work was conducted within the funding measure "Regional information for action on climate change" (RegIKlim) of the German Federal Ministry of Education and Research (BMBF) in the ISAP project (01LR2007B & 01LR2007B1) and the NUKLEUS project (01LR2002B & 01LR2002B1), as well as in ClimXtreme 2 (01LP2322A). Joaquim G. Pinto was supported by the AXA Research Fund. Hayley J. Fowler was supported by the Climate+ Co-Centre funded by UKRI (NE/Y006496/1) and by IMPETUS4CHANGE funded by HORIZON-CL5-2022-D1-02 (Grant agreement ID: 101081555) and the UKRI Horizon Europe Guarantee (10047737). We thank Hans-Jürgen Panitz and Regina Kohlhepp for performing the COSMO-CLM simulations. The simulations were performed on the national supercomputers Cray XC40 Hazel Hen and HPE Apollo Hawk at the High Performance Computing Centre Stuttgart (project HRCM ID-12801). Parts of the processing were performed at DKRZ. Observational data was provided by Deutscher Wetterdienst. We thank Roberto Villalobos Herrera (University of Costa Rica) for valuable discussions.

Appendix A. Supplementary data

Supplementary material related to this article can be found online at https://doi.org/10.1016/j.wace.2025.100764.

Data availability

Station data and the radar dataset are available from Deutscher Wetterdienst (https://opendata.dwd.de/climate_environment/CDC, last access February 2024). Simulation data from the KIT-KLIWA ensemble are available on request from the authors.

References

Archer, D.R., Fowler, H.J., 2018. Characterising flash flood response to intense rainfall and impacts using historical information and gauged data in Britain. J. Flood Risk Manag. 11, S121–S133. http://dx.doi.org/10.1111/jfr3.12187.

Ban, N., Caillaud, C., Coppola, E., Pichelli, E., Sobolowski, S., Adinolfi, M., Ahrens, B., Alias, A., Anders, I., Bastin, S., et al., 2021. The first multi-model ensemble of regional climate simulations at kilometer-scale resolution, part I: evaluation of precipitation. Clim. Dyn. 57, 275–302. http://dx.doi.org/10.1007/s00382-021-05708-w.

Ban, N., Schmidli, J., Schär, C., 2014. Evaluation of the convection-resolving regional climate modeling approach in decade-long simulations. J. Geophys. Res.: Atmos. 119 (13), 7889–7907. http://dx.doi.org/10.1002/2014JD021478.

Ban, N., Schmidli, J., Schär, C., 2015. Heavy precipitation in a changing climate: Does short-term summer precipitation increase faster? Geophys. Res. Lett. 42 (4), 1165–1172. http://dx.doi.org/10.1002/2014GL062588.

Bartels, H., Weigl, E., Reich, T., Lang, P., Wagner, A., Kohler, O., Gerlach, N., 2004. Projekt RADOLAN-Routineverfahren zur Online-Aneichung der Radarniederschlagsdaten mit Hilfe von automatischen Bodenniederschlagsstationen (Ombrometer): zusammenfassender Abschlussbericht für die Projektlaufzeit von 1997 bis 2004. Technical Report, Deutscher Wetterdienst.

Brisson, E., Demuzere, M., Van Lipzig, N., 2015. Modelling strategies for performing convection-permitting climate simulations. Meteorol. Z. 25 (2), 149–163. http://dx.doi.org/10.1127/metz/2015/0598.

Chan, S.C., Kendon, E.J., Roberts, N.M., Fowler, H.J., Blenkinsop, S., 2016. The characteristics of summer sub-hourly rainfall over the southern UK in a high-resolution convective permitting model. Environ. Res. Lett. 11 (9), 094024. http://dx.doi.org/10.1088/1748-9326/11/9/094024.

Darwish, M.M., Fowler, H.J., Blenkinsop, S., Tye, M.R., 2018. A regional frequency analysis of UK sub-daily extreme precipitation and assessment of their seasonality. Int. J. Climatol. 38 (13), 4758–4776. http://dx.doi.org/10.1002/joc.5694.

Fosser, G., Khodayar, S., Berg, P., 2015. Benefit of convection permitting climate model simulations in the representation of convective precipitation. Clim. Dyn. 44, 45–60. http://dx.doi.org/10.1007/s00382-014-2242-1.

Hackenbruch, J., Schädler, G., Schipper, J.W., 2016. Added value of high-resolution regional climate simulations for regional impact studies. Meteorol. Z. 25 (3), 291–304. http://dx.doi.org/10.1127/metz/2016/0701.

Helsen, S., van Lipzig, N.P., Demuzere, M., Vanden Broucke, S., Caluwaerts, S., De Cruz, L., De Troch, R., Hamdi, R., Termonia, P., Van Schaeybroeck, B., et al., 2020. Consistent scale-dependency of future increases in hourly extreme precipitation in two convection-permitting climate models. Clim. Dyn. 54 (3), 1267–1280. http://dx.doi.org/10.1007/s00382-019-05056-w.

Hettiarachchi, S., Wasko, C., Sharma, A., 2018. Increase in flood risk resulting from climate change in a developed urban watershed–the role of storm temporal patterns. Hydrol. Earth Syst. Sci. 22 (3), 2041–2056. http://dx.doi.org/10.5194/hess-22-2041-2018.

Hohenegger, C., Brockhaus, P., Schär, C., 2008. Towards climate simulations at cloud-resolving scales. Meteorol. Z. 17 (4), 383–394. http://dx.doi.org/10.1127/0941-2948/2008/0303.

Hundhausen, M., Feldmann, H., Kohlhepp, R., Pinto, J.G., 2024. Climate change signals of extreme precipitation return levels for Germany in a transient convection-permitting simulation ensemble. Int. J. Climatol. http://dx.doi.org/10.1002/joc.8393.

Hundhausen, M., Feldmann, H., Laube, N., Pinto, J.G., 2023. Future heat extremes and impacts in a convection-permitting climate ensemble over Germany. Nat. Hazards Earth Syst. Sci. 23 (8), 2873–2893. http://dx.doi.org/10.5194/nhess-23-2873-2023.

Kendon, E.J., Roberts, N.M., Senior, C.A., Roberts, M.J., 2012. Realism of rainfall in a very high-resolution regional climate model. J. Clim. 25 (17), 5791–5806. http://dx.doi.org/10.1175/JCLI-D-11-00562.1.

Lambourne, J.J., Stephenson, D., 1987. Model study of the effect of temporal storm distributions on peak discharges and volumes. Hydrol. Sci. J. 32 (2), 215–226. http://dx.doi.org/10.1080/02626668709491179.

Meredith, E.P., Ulbrich, U., Rust, H.W., 2020. Subhourly rainfall in a convection-permitting model. Environ. Res. Lett. 15 (3), 034031. http://dx.doi.org/10.1088/1748-9326/ab6787.

Müller, S.K., Caillaud, C., Chan, S., De Vries, H., Bastin, S., Berthou, S., Brisson, E., Demory, M.-E., Feldmann, H., Goergen, K., et al., 2023. Evaluation of Alpine-Mediterranean precipitation events in convection-permitting regional climate models using a set of tracking algorithms. Clim. Dyn. 61 (1–2), 939–957. http://dx.doi.org/10.1007/s00382-022-06555-z.

Müller, T., Schütze, M., Bárdossy, A., 2017. Temporal asymmetry in precipitation time series and its influence on flow simulations in combined sewer systems. Adv. Water Resour. 107, 56–64. http://dx.doi.org/10.1016/j.advwatres.2017.06.010.

Ng, J.Y., Fazlollahi, S., Galelli, S., 2020. Do design storms yield robust drainage systems? How rainfall duration, intensity, and profile can affect drainage performance. J. Water Resour. Plan. Manag. 146 (3), 04020003. http://dx.doi.org/10.1061/(ASCE)WR.1943-5452.0001167.

Pichler, M., 2024. idf_analysis: Intensity duration frequency analysis with python based on KOSTRA. http://dx.doi.org/10.5281/ZENODO.10559992.

Piper, D., Kunz, M., Ehmele, F., Mohr, S., Mühr, B., Kron, A., Daniell, J., 2016. Exceptional sequence of severe thunderstorms and related flash floods in May and June 2016 in Germany–Part 1: Meteorological background. Nat. Hazards Earth Syst. Sci. 16 (12), 2835–2850. http://dx.doi.org/10.5194/nhess-16-2835-2016.

Prein, A.F., Gobiet, A., Suklitsch, M., Truhetz, H., Awan, N.K., Keuler, K., Georgievski, G., 2013. Added value of convection permitting seasonal simulations. Clim. Dyn. 41, 2655–2677. http://dx.doi.org/10.1007/s00382-013-1744-6.

Prein, A.F., Langhans, W., Fosser, G., Ferrone, A., Ban, N., Goergen, K., Keller, M., Tölle, M., Gutjahr, O., Feser, F., et al., 2015. A review on regional convection-permitting climate modeling: Demonstrations, prospects, and challenges. Rev. Geophys. 53 (2), 323–361. http://dx.doi.org/10.1002/2014RG000475.

Rajczak, J., Schär, C., 2017. Projections of future precipitation extremes over Europe: A multimodel assessment of climate simulations. J. Geophys. Res.: Atmos. 122 (20), 10–773. http://dx.doi.org/10.1002/2017JD027176.

Restrepo-Posada, P.J., Eagleson, P.S., 1982. Identification of independent rainstorms. J. Hydrol. 55 (1–4), 303–319. http://dx.doi.org/10.1016/0022-1694(82)90136-6.

Rockel, B., Will, A., Hense, A., 2008. The Regional Climate Model COSMO-CLM (CCLM). Meteorol. Z. 17 (4), 347–348. http://dx.doi.org/10.1127/0941-2948/2008/0309.

Sato, T., Miura, H., Satoh, M., Takayabu, Y.N., Wang, Y., 2009. Diurnal cycle of precipitation in the tropics simulated in a global cloud-resolving model. J. Clim. 22 (18), 4809–4826. http://dx.doi.org/10.1175/2009JCLI2890.1.

Tiedtke, M., 1989. A comprehensive mass flux scheme for cumulus parameterization in large-scale models. Mon. Weather Rev. 117 (8), 1779–1800. http://dx.doi.org/10.1175/1520-0493(1989)117<1779:ACMFSF>2.0.CO;2.

Vergara-Temprado, J., Ban, N., Schär, C., 2021. Extreme sub-hourly precipitation intensities scale close to the Clausius-Clapeyron rate over Europe. Geophys. Res. Lett. 48 (3), http://dx.doi.org/10.1029/2020GL089506, e2020GL089506.

Villalobos Herrera, R., Blenkinsop, S., Guerreiro, S.B., Dale, M., Faulkner, D., Fowler, H.J., 2023a. Towards new design rainfall profiles for the United Kingdom. J. Flood Risk Manag. e12958. http://dx.doi.org/10.1111/jfr3.12958.

Villalobos Herrera, R., Blenkinsop, S., Guerreiro, S.B., Fowler, H.J., 2023b. The creation and climatology of a large independent rainfall event database for Great Britain. Int. J. Climatol. 43 (13), 6020–6037. http://dx.doi.org/10.1002/joc.8187.

Visser, J.B., Wasko, C., Sharma, A., Nathan, R., 2023. Changing storm temporal patterns with increasing temperatures across Australia. J. Clim. 1–26. http://dx.doi.org/10.1175/JCLI-D-22-0694.1.

Wasko, C., Sharma, A., 2015. Steeper temporal distribution of rain intensity at higher temperatures within Australian storms. Nat. Geosci. 8 (7), 527–529. http://dx.doi.org/10.1038/ngeo2456.

Zhu, Z., Wright, D.B., Yu, G., 2018. The impact of rainfall space-time structure in flood frequency analysis. Water Resour. Res. 54 (11), 8983–8998. http://dx.doi.org/10.1029/2018WR023550.